STEM CELLS AND DEVELOPMENT
Volume 27, Number 2, 2018

DOI: 10.1089/scd.2017.0139

DYRK1A Is a Regulator of S-Phase Entry in Hepatic Progenitor Cells

Hedwig S. Kruitwagen,[1] Bart Westendorp,[2] Cornelia S. Viebahn,[1] Krista Post,[1] Monique E. van Wolferen,[1] Loes A. Oosterhoff,[1] David A. Egan,[3] Jean-Maurice Delabar,[4,5] Mathilda J. Toussaint,[2] Baukje A. Schotanus,[1] Alain de Bruin,[2] Jan Rothuizen,[1] Louis C. Penning,[1,*] and Bart Spee[1,*]

Hepatic progenitor cells (HPCs) are adult liver stem cells that act as second line of defense in liver regeneration. They are normally quiescent, but in case of severe liver damage, HPC proliferation is triggered by external activation mechanisms from their niche. Although several important proproliferative mechanisms have been described, it is not known which key intracellular regulators govern the switch between HPC quiescence and active cell cycle. We performed a high-throughput kinome small interfering RNA (siRNA) screen in HepaRG cells, a HPC-like cell line, and evaluated the effect on proliferation with a 5-ethynyl-2′-deoxyuridine (EdU) incorporation assay. One hit increased the percentage of EdU-positive cells after knockdown: dual specificity tyrosine phosphorylation regulated kinase 1A (*DYRK1A*). Although upon *DYRK1A* silencing, the percentage of EdU- and phosphorylated histone H3 (pH3)-positive cells was increased, and total cell numbers were not increased, possibly through a subsequent delay in cell cycle progression. This phenotype was confirmed with chemical inhibition of DYRK1A using harmine and with primary HPCs cultured as liver organoids. DYRK1A inhibition impaired Dimerization Partner, RB-like, E2F, and multivulva class B (DREAM) complex formation in HPCs and abolished its transcriptional repression on cell cycle progression. To further analyze *DYRK1A* function in HPC proliferation, liver organoid cultures were established from mBACtgDyrk1A mice, which harbor one extra copy of the murine *Dyrk1a* gene (*Dyrk*+++). *Dyrk*+++ organoids had both a reduced percentage of EdU-positive cells and reduced proliferation compared with wild-type organoids. This study provides evidence for an essential role of *DYRK1A* as balanced regulator of S-phase entry in HPCs. An exact gene dosage is crucial, as both *DYRK1A* deficiency and overexpression affect HPC cell cycle progression.

Keywords: *DYRK1A*, cell cycle, hepatic progenitor cells, proliferation, RNA interference screen

Introduction

The liver is well known for its regenerative capacity, which is primarily based on hepatocyte replication [1,2]. This first line of defense fails, however, in cases of fulminant or chronic liver injury [3–5]. Liver repair then relies on hepatic progenitor cells (HPCs). HPCs are adult liver stem cells that are normally quiescent, but start to proliferate upon severe hepatic damage and can differentiate into mature hepatocytes [6–10]. In practice, this HPC-response is often still insufficient for clinical recovery of liver disease [11].

Adult stem cells require a well-regulated balance between quiescence and cell cycle entry to prevent premature exhaustion while maintaining self-renewal capacity [12]. Proliferation is initiated by specific cues from their tissue microenvironment or niche [13]. For HPCs, several external activation mechanisms have been described, such as Wnt signaling, growth factors and cytokines (eg, hepatocyte growth factor, TNF-like weak inducer of apoptosis [TWEAK]), and specific extracellular matrix components [14–17].

However, it is not known which key intracellular regulators downstream of these external signals govern the

Departments of [1]Clinical Sciences of Companion Animals and [2]Pathobiology, Faculty of Veterinary Medicine, Utrecht University, Utrecht, the Netherlands.
[3]Department of Cell Biology, Centre for Molecular Medicine, UMC Utrecht, Utrecht, the Netherlands.
[4]Université Paris Diderot, Sorbonne Paris Cité, Unité de Biologie Fonctionnelle et Adaptative (BFA), UMR 8251 CNRS, F-75205, Paris, France.
[5]Brain & Spine Institute (ICM) CNRS UMR7225, INSERM UMRS 975, Paris, France.
*Both authors contributed equally to this work.

switch between quiescence and active cell cycle in HPCs. Identification of these essential determinants of the HPC-response could give greater insight into the biology behind HPC-mediated liver regeneration and could lead to new therapeutic strategies for patients with severe liver disease.

In this study, we therefore aimed to screen for kinases that are essential in HPC proliferation. Kinases are known for their involvement in the cell cycle and proliferation [18–20]. As a class, they are commonly exploited as drug targets, with many (receptor tyrosine) kinase inhibitors already in use in the clinic. To this end, we used a kinase siRNA library in HepaRG cells, a HPC-like cell line, and studied the effect on the cell cycle with a 5-ethynyl-2′-deoxyuridine (EdU) incorporation assay (a detailed screening strategy is summarized in Fig. 1). The kinome screen generated one hit: dual-specificity tyrosine phosphorylation-regulated kinase 1A (*DYRK1A*). To validate our findings, we confirmed the observed phenotype in primary HPCs cultured as liver organoids [21] and also investigated an overexpression model with one extra copy of the *DYRK1A* gene [22].

Materials and Methods

Culture of HepaRG cell line

Human hepatic progenitor-like cell line HepaRG was obtained from Biopredic International (Rennes, France). Human hepatic stellate cell line LX2 was kindly provided by Scott Friedman (Mount Sinai School of Medicine, New York, NY). Cells were cultured in William's Medium E with 2% v/v fetal calf serum (Life Technologies), 5 μg/mL insulin, 50 μM hydrocortisone hemisuccinate (Sigma-Aldrich), and standard antibiotics at 37°C in 5% CO_2 in air in a humidified incubator.

High-throughput siRNA screen, immunofluorescence, and image acquisition

A Dharmacon On-Target-Plus siRNA library (Thermo Scientific) targeting 716 kinases in the human genome was used in the primary screen. A transfection protocol was developed that yielded more than 90% transfection efficiency and knockdown without affecting viability or cell loss (<10%). siRNAs were forward transfected in 5,500 HepaRG cells/well (confluency of 30%) in 96-well plates in triplicate at a concentration of 5 nM using 3 μL/mL RNAiMAX transfection reagent (Thermo Scientific) in antibiotic-free media. As controls, nontargeting (NT) siRNAs and SMARTpool siRNAs against BMI1 proto-oncogene, polycomb ring finger (*BMI1*), and polo-like kinase 1 (*PLK1*) were used. Cells were cultured for 48 h in total after transfection. After 24 h, transfection medium was removed and replaced with standard culture medium with antibiotics. After 48 h, cells were pulsed in culture with 10 μM EdU for 3 h, then washed with phosphate-buffered saline (PBS) with 0.1% Tween, and fixed and permeabilized with 4% paraformaldehyde (PFA) and 0.5% Triton X-100 for 10 min at room temperature (RT). Fixative was replaced with PBS, and cells were stained for EdU and phosphorylated histone H3 (pH3), using a Sciclone automated workstation (Caliper Life Sciences).

EdU staining was performed with 5 μM AF488-azide (Thermo Scientific), 1 mM $CuSO_4$, and 100 mM ascorbic acid according to Salic and Mitchison [23]. For pH3 staining, cells were blocked with 5% v/v normal goat serum (Sigma-Aldrich) and then incubated with rabbit anti-pH3 (1:500, 06-570, lot No. 1957281; Millipore) for 1 h. Cells were washed and then incubated with goat anti-rabbit AF568 (1:200; Life Technologies) for 1 h. Cells were washed and nuclei were counterstained with 4′,6-diamidino-2-phenylindole (DAPI; Sigma-Aldrich). Total cell count and the percentages of EdU- and pH3-positive cells were calculated with automated image acquisition and data analysis using the Target Activation algorithm of the Cellomics ArrayScan VTI HCS Reader (Thermo Scientific).

Screening strategy, data normalization, and hit selection

The screening strategy is summarized in Fig. 1. In a primary screen, all 716 kinases in the library were screened in triplicate in HepaRG cells using a pool of 4 siRNAs per target. After 48 h, the percentage of EdU was determined. Data were normalized with a robust *Z* score analysis (sample-based normalization), and a significance threshold of 3 was established mathematically by Monte Carlo analysis [24]. Consequently, hits were defined as having a robust *Z* score of either ≥3 (increased percentage of EdU-positive cells after silencing) or ≤−3 (decreased percentage of EdU-positive cells after silencing) in at least two out of three replicates.

Obtained hits were reanalyzed in a secondary screen with a randomized plate setup and including 10 NT control siRNAs per plate. Transfections were performed in plate triplicates to control for interplate variation. In addition, the secondary screen included a second cell line as negative selector to rule out common, non-HPC-specific hits. For this purpose, the hepatic stellate cell line LX2 was selected, representing liver cells of a different (mesenchymal) lineage. Assuming a biased population in this confirmatory screen, a control-based hit selection was used, with two standard deviations away from the NT controls as cutoff. A target had to be a hit in at least two out of three replicate plates.

Remaining hits were technically validated in a deconvolution screen in HepaRG cells, individually transfecting four single siRNAs per target to control for off-target effects. Hit selection was similar as in the secondary screen, with the

FIG. 1. High-throughput screen strategy. **(A)** In a primary screen, 716 kinases were screened using a pool of 4 siRNAs per target. Transfections were performed in triplicate. After 48 h, cells were pulsed with EdU, stained, and percentage of EdU^+ cells was determined with automated image analysis. Hits were selected based on sample-based normalization. **(B)** Secondary screen included a non-HPC cell line (LX2). Transfections were performed in triplicate. Per plate 10 NT controls distributed at random across the plate were used for control-based hit selection. **(C)** Deconvolution using four single siRNAs per target (at least two had to yield hit phenotype) and control-based hit selection. RNA was isolated to confirm knockdown of the target. Transfections were performed in triplicate for both EdU assay and RNA isolation. EdU, 5-ethynyl-2′-deoxyuridine; HPC, hepatic progenitor cell; NT, nontargeting; siRNA, small interfering RNA. Color images available online at www.liebertpub.com/scd

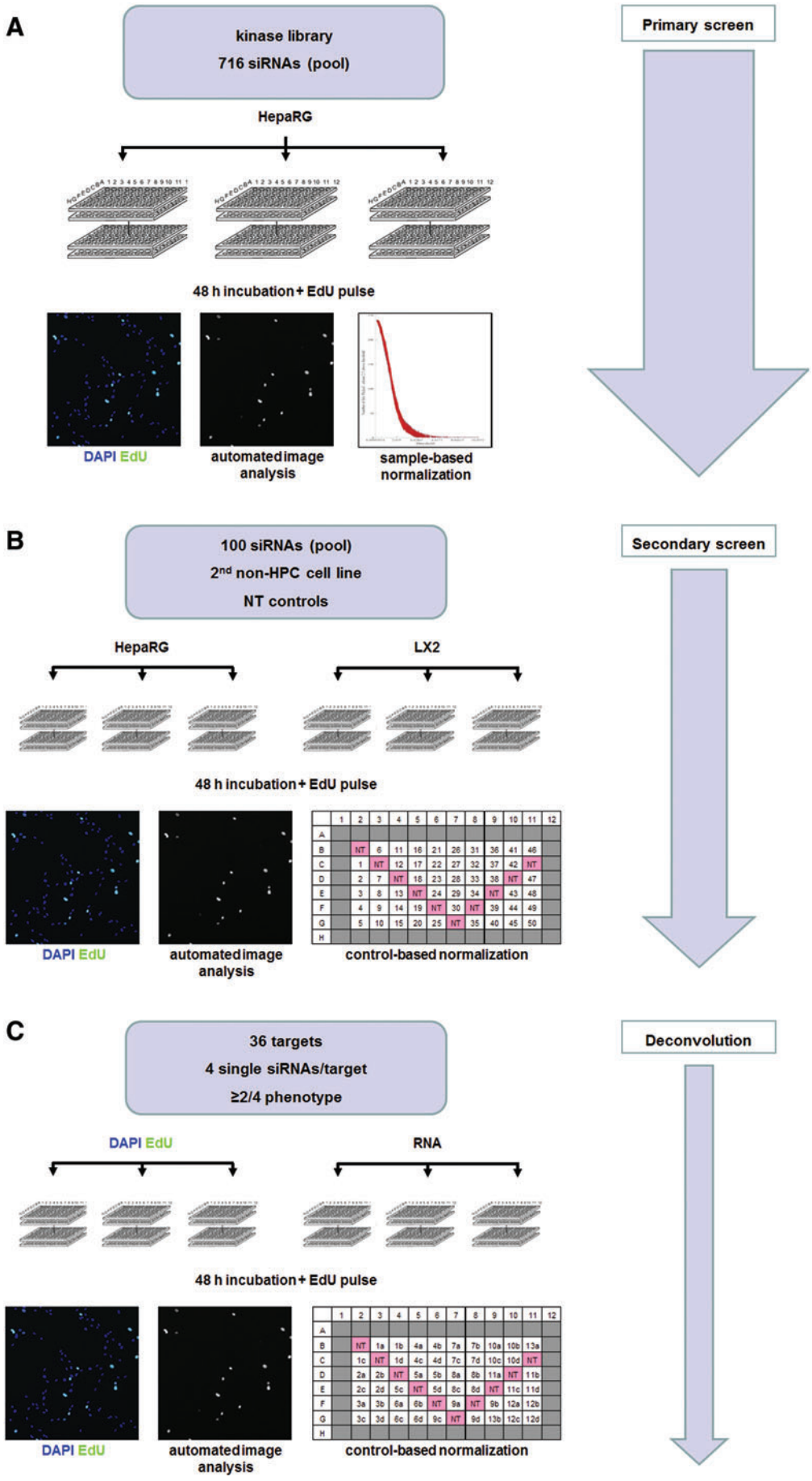

added requirement that at least two out of four siRNAs had to produce a hit phenotype. In the same transfection experiment, RNA was isolated in triplicate to confirm knockdown of the target [25].

RNA isolation and quantitative reverse transcriptase polymerase chain reaction analysis

RNA was isolated with either sample preparation reagent (BioRad) or an RNeasy kit (Qiagen) from three to six culture replicates. Complementary DNA (cDNA) reaction and quantitative polymerase chain reaction (qPCR) were performed in duplicate essentially as described before [26] on a Bio-Rad CFX thermal cycler (Bio-Rad). Primers were designed for human and mouse *DYRK1A/Dyrk1a*, mouse E2f transcription factor 1 (*E2f1*), cell division cycle 6 (*Cdc6*), proliferating cell nuclear antigen (*Pcna*), cyclin B1 (*Ccnb1*), *Plk1*, epithelial cell transforming 2 (*Ect2*), and cyclin-dependent kinase inhibitor 1B (*Cdkn1b*). Gene expression was normalized against reference genes (human: *HPRT* and *RPL19*, mouse: *β-Actin*, *Rps18*, and *Gapdh*). Primers are listed in Table 1.

Protein isolation and western blotting

Total protein was isolated from HepaRG cells cultured in a six-well plate (165,000 cells/well). Protein isolation and western blotting were performed essentially as described before [26]. For LIN52 immunoblotting, dephosphorylation of samples (100 μg protein) was performed with 100 U lambda protein phosphatase (λPP; New England Biolabs) in 1×NEBuffer for protein metallo phosphatases (PMP), supplemented with 1 mM $MnCl_2$ at 30°C for 30 min. For DYRK1A immunoblotting, polyclonal antibody against DYRK1A (HPA015810, lot No. A71674; Sigma-Aldrich) was diluted 1:250, and secondary goat anti-rabbit antibody (Dako) was diluted 1:5,000. As a loading control, β-actin antibody (MS1295P1, lot No. 1295P1501P; Thermo Scientific) was used in a 1:2,000 dilution. For LIN52 immunoblotting, polyclonal antibody against LIN52 (HPA000900, lot No. A79391; Sigma-Aldrich) was diluted 1:100 and secondary goat anti-rabbit antibody (Cell Signaling) was diluted 1:3,000. As a loading control, alpha-tubulin antibody (T6199, lot No. 102M4773V; Sigma-Aldrich) was used in a 1:1,000 dilution. Quantification was performed using Quantity one (Version 4.6.9; Bio-Rad). Sample p-LIN52 was quantified as optical density per mm^2 and normalized against alpha-tubulin. Omission of the first antibody was used as negative control.

Flow cytometry and cell cycle distribution analysis

HepaRG cells 48 h after transfection with either NT control or siRNA against *DYRK1A* were harvested by enzymatic digestion and fixed in 70% ethanol at 4°C overnight. Cells were stained with 5 μg/mL propidium iodide and 250 μg/mL RNase in PBS. For flow cytometry a FACSCalibur (BD Biosciences) was used. Acquired DNA content data were analyzed with FlowJo software for cell cycle distribution (curve fit according to Dean Jett Fox model). DNA content

Table 1. Primer Sequences and Quantitative Polymerase Chain Reaction Conditions

Species	*Gene*	*Direction*	*Sequence (5′–3′)*	*Temperature (°C)*	*Product size (bp)*
Human	*DYRK1A*	Forward	TTGACTCCTTGATAGGCAAAGGT	60	70
		Reverse	CATTCTTGCTCCACACGATCAT		
	HPRT	Forward	ATAAGCCAGACTTTGTTGGA	60	156
		Reverse	CTCAACTTGAACTCTCATCTTAGG		
	RPL19	Forward	ATGAGTATGCTCAGGCTTCAG	64	150
		Reverse	GATCAGCCCATCTTTGATGAG		
Mouse	*Dyrk1a*	Forward	GTGTCTGCCTTACCATATTCTG	61	83
		Reverse	TGCTGGATCACGGAAGG		
	E2f1	Forward	GCCCTTGACTATCACTTTGGTCTC	64	270
		Reverse	CCTTCCCATTTTGGTCTGCTC		
	Cdc6	Forward	AGTTCTGTGCCCGCAAAGTG	63	289
		Reverse	AGCAGCAAAGAGCAAACCAGG		
	Pcna	Forward	TGAAGATAATGCAGACACCTTAGC	61	124
		Reverse	TGTACTCCTGTTCTGGGATTCC		
	Ccnb1	Forward	AAAGGGAAGCAAAAACGCTAGG	59	130
		Reverse	TGTTCAAGTTCAGGTTCAGGCTC		
	Plk1	Forward	CCAAGCACATCAACCCAGTG	60	147
		Reverse	TGAGGCAGGTAATAGGGAGACG		
	Ect2	Forward	AGAGACGGAGATTGAAAGAGACC	60	110
		Reverse	GTGAGCCAATAGAAAGAGAGTGC		
	Cdkn1b	Forward	GGTGCCTTTAATTGGGTCTCAG	61	140
		Reverse	AAGAAGAATCTTCTGCAGCAGG		
	β-Actin	Forward	AGCTCCTTCGTTGCCGGTCCA	57	94
		Reverse	TTTGCACATGCCGGAGCCGTTG		
	Rps18	Forward	GATCCCTGAGAAGTTCCAGCAC	57	120
		Reverse	ACCACATGAGCATATCTCCGC		
	Gapdh	Forward	GAAGGTCGGTGTGAACGG	61	101
		Reverse	TGAAGGGGTCGTTGATGG		

Ccnb1, cyclin B1; *Cdc6*, cell division cycle 6; *Cdkn1b*, cyclin-dependent kinase inhibitor 1B; *DYRK1A*, dual-specificity tyrosine phosphorylation-regulated kinase 1A; *E2f1*, E2f transcription factor 1; *Ect2*, epithelial cell transforming 2; *Pcna*, proliferating cell nuclear antigen; *Plk1*, polo-like kinase 1.

data (DAPI total intensity) from the ArrayScan automated image acquisition were similarly analyzed with FlowJo.

Chemical DYRK1A inhibition

Harmine is a specific DYRK1A inhibitor [27,28]. HepaRG cells and liver organoids were treated with 10 μM harmine (Sigma-Aldrich) or its vehicle (dimethyl sulfoxide [DMSO]) control for 48 h for EdU, pH3, trypan blue exclusion, and terminal deoxynucleotidyl transferase dUTP nick end labeling (*TUNEL*) assays. Medium was refreshed after 24 h. Growth curves were made by trypsinization and cell counts upon treatment with 10 μM harmine, 15 μM INDY, and 6.7 μM GNF7156 or their vehicle (DMSO) control. TUNEL staining was performed according to the manufacturer's instructions (Merck Millipore). Ten high-power fields were counted per condition.

Mouse liver organoid culture

Surplus mouse liver samples were obtained from 14 to 20 weeks old wild-type (WT) and mBACtgDyrk1A mice ($n=5$ transgenic and $n=4$ WT littermates) killed for unrelated research purposes (University 3R-policy). mBACtgDyrk1A mice were generated as described previously and contain one extra copy of the murine *Dyrk1a* gene [22]. Liver samples were processed fresh or immediately frozen in cryopreservative (Life Technologies). Liver was minced and then digested with 125 μg/mL collagenase type XI (Sigma-Aldrich) and 125 μg/mL dispase (Life Technologies) to obtain biliary duct fragments containing the HPCs. Ducts were seeded in three-dimensional (3D) culture in Matrigel (BD Biosciences) in 48- or 24-well plates and overlaid with expansion media. Primary HPCs proliferated in response to the Wnt ligands in the defined media as 3D liver organoids as described before [21]. Imaging was performed with an Olympus microscope (CKX41) and a Leica DFC425C camera.

EdU incorporation assay in organoids

Organoids from passage 5 onward in log phase of growth were pulsed with 10 μM of EdU for 3 h, fixed in 4% PFA, and embedded in paraffin. Organoid sections of 4 μm were routinely dewaxed and rehydrated and stained for EdU as described before and nuclei were counterstained with DAPI. Sections were imaged with an Olympus IMT-2 fluorescence microscope and an Olympus E-330 LCD camera. For at least 2,000 cells per condition, total cell number and number of EdU^+ cells were counted.

Organoid growth curves

To quantify liver organoid growth, organoids were cultured in 48-well plates ($n=4$ wells per condition) and an Alamar Blue assay was performed on the same wells on 5 consecutive days according to the manufacturer's instructions (Life Technologies). Serial fluorescence measurements were made on a Tecan Infinite M200 spectrophotometer and were normalized to day 1.

Organoid γH2AX immunocytochemistry

Paraffin-embedded organoid sections of 4 μm were routinely dewaxed and rehydrated and incubated in 10 mM citrate at 98°C for 30 min with an additional 30 min cooling down. Endogenous peroxidase activity was blocked with 0.3% H_2O_2 in methanol. Sections were washed with PBS containing 0.1% Tween and incubated with 10% v/v normal goat serum (Sigma-Aldrich) for 30 min at RT. Sections were incubated with rabbit anti-γH2AX (1:500, MABE205, clone EP854(2)Y, lot No. 2452454; Millipore) at 4°C overnight. Sections were incubated with goat anti-rabbit (Envision; Dako) for 45 min at RT, and 3,3′diaminobenzidine was used as chromogen. Hematoxylin was used as counterstain. Imaging was performed with an Olympus microscope (CKX41) and a Leica DFC425C camera, at least 1,000 nuclei were counted per condition.

Statistics

Statistical significance was determined using a nonparametric Mann–Whitney U test or a Kruskal–Wallis test followed by a Mann–Whitney U test in case of multiple group testing, $P \leq 0.05$ was considered significant. Analysis was performed in SPSS (IBM SPSS Statistics 22).

Results

RNA interference screening of kinase library in HepaRG cell line

In a primary screen, 716 kinases were silenced and screened for their effect on EdU incorporation in the HepaRG cell line. After normalization, 100 hits were identified based on a robust *Z* score of either ≥3 (increased percentage of EdU-positive cells after silencing) or ≤–3 (decreased percentage of EdU positive cells after silencing) (Fig. 2A). As confirmation that our screen was robust, siRNAs against two essential kinases (*BMI1* and *PLK1*) consistently yielded *Z* scores of <–3, and NT controls did not yield a hit phenotype.

The obtained hits were reanalyzed in a secondary screen in triplicate and, as a biological validation, tested in parallel for their effect in a non-HPC liver cell line (LX2, stellate cell line) to rule out non-HPC-specific hits. The secondary screen validated 41 hits, of which 36 were unique for HepaRG cells and did not yield a similar phenotype in LX2 cells.

To control for potential off-target effects, a deconvolution screen was performed using single siRNAs, and knockdown was confirmed on messenger RNA (mRNA) level by qPCR (data not shown for all hits). In total 10 hits were confirmed with at least 2 out of 4 siRNAs producing a phenotype (Fig. 2B, overview of screen hit confirmation in Fig. 2C). Out of these 10 hits, only 1 hit resulted in an increase in percentage of EdU-positive cells after silencing. This kinase was identified as *DYRK1A*. *DYRK1A* is an important regulator of proliferation of neural progenitor cells and pancreatic β cells [29–31]. However, its role in HPCs is unexplored and is a subject of further investigation.

Effect of DYRK1A silencing in HepaRG cell line on percentage of EdU^+ cells, percentage of $pH3^+$ cells, and proliferation

We first confirmed that siRNA-mediated gene silencing of *DYRK1A* in HepaRG cells resulted in a 97% knockdown on mRNA level and 65% on protein level after 48 h (Fig. 3A). Consistent with the results from our screen, *DYRK1A* silencing significantly increased the percentage of of EdU^+ and $pH3^+$ cells (Fig. 3B, C), suggesting more cells entered S phase and G2/M phase of the cell cycle. However, we did not observe

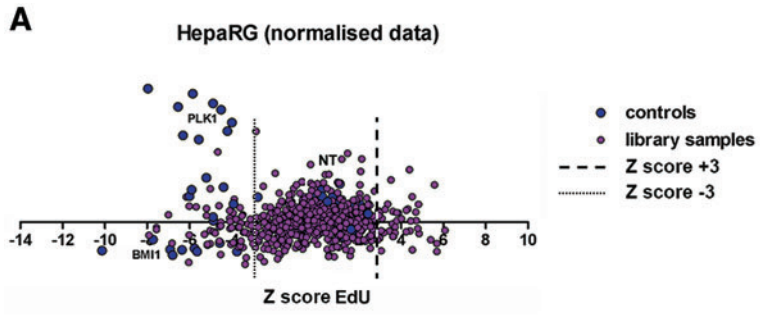

B

Kinase	Accession nr.	#siRNAs	Phenotype % EdU+
DYRK1A	NM_130438	2/4	increased
TNNI3K	NM_015978	4/4	decreased
PRKAR1A	NM_002734	3/4	decreased
ITPKA	NM_002220	2/4	decreased
C9ORF12	NM_022755	2/4	decreased
PIP5K1B	NM_003558	2/4	decreased
PCTK1	NM_006201	2/4	decreased
GCK	NM_033507	2/4	decreased
PIK3CB	NM_006219	2/4	decreased
RPS6KC1	NM_012424	2/4	decreased

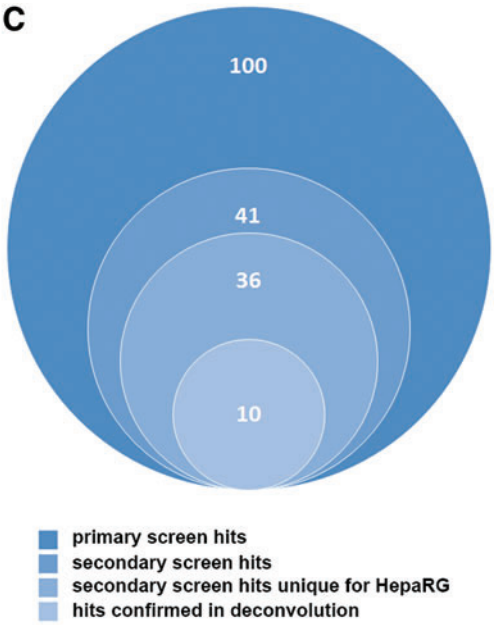

FIG. 2. RNAi screen hits in HepaRG cell line. **(A)** Scatter plot representing robust *Z* scores in the primary screen. Out of 716 screened kinases, 100 hits were selected based on a robust *Z* score of either ≥3 (increased percentage of EdU^+ cells after silencing) or ≤−3 (decreased percentage of EdU^+ cells after silencing). siRNAs against BMI1 and PLK1 (essential kinases) were used as controls. **(B)** Final hit list. Deconvolution screening validated 10 hits with ≥2 out of 4 siRNAs producing a phenotype. **(C)** Schematic representation of screen hit confirmation. BMI1, BMI1 proto-oncogene, polycomb ring finger; PLK1, polo-like kinase 1; RNAi, RNA interference. Color images available online at www.liebertpub.com/scd

significant changes in total cell numbers after 48 h of *DYRK1A* silencing (Fig. 3C). Cell cycle distribution analysis of ArrayScan DNA content data with FlowJo software showed that upon *DYRK1A* gene silencing the population of cells in S and G2 phase of the cell cycle was increased (Fig. 3D). This phenotype was confirmed by flow cytometry (Fig. 3E).

Validation of phenotype in HepaRG cell line with chemical DYRK1A inhibitor

We tested whether the phenotype could be recapitulated with harmine, a specific chemical inhibitor of DYRK1A [27,28]. Harmine treatment similarly increased the percentage of EdU^+ and $pH3^+$ cells compared with vehicle control (Fig. 3F). However, proliferation did not increase upon incubation with harmine nor with other DYRK1A inhibitors INDY and GNF7156 (Fig. 3G). Rather a trend for growth arrest was observed. Chemical DYRK1A inhibition did not affect cellular viability as measured by trypan blue exclusion and TUNEL staining assays (Fig. 3H). We concluded that DYRK1A silencing/inhibition enhances progression through the cell cycle but does not enhance cell division. An explanation for these findings could be that DYRK1A enhances S-phase entry of cells at the expense of a subsequent

FIG. 3. Effects of DYRK1A silencing and chemical inhibition on HepaRG cell cycle. **(A)** Knockdown of DYRK1A after 48 h on mRNA (97%) and protein level (65%). β-actin served as loading control. **(B)** Representative images of DAPI (*blue*), EdU (*green*), and pH3 (*red*) immunofluorescent staining after either NT control or siRNA against *DYRK1A* (siDYRK1A) transfection. Scale bars indicate 100 μm. **(C)** *Dot* plots representing percentages of EdU^+ and $pH3^+$ cells and total cell count after either NT or siDYRK1A transfection. **(D)** Cell cycle distribution analysis (FlowJo) of total DAPI staining intensity per nucleus and scatterplots of DAPI versus EdU staining intensity per nucleus after either NT or siDYRK1A transfection. **(E)** Flow cytometry analysis of cell cycle distribution using PI as measure of DNA content. **(F)** *Dot* plots representing percentages of EdU^+ and $pH3^+$ cells after 48 h of treatment with either vehicle or harmine. **(G)** Growth curve of HepaRG cells treated with vehicle, harmine, INDY, or GNF7156 for 6 days. **(H)** Representative phase contrast images of HepaRG cells after 48 h of treatment with vehicle, harmine, INDY, or GNF7156. Scale bars indicate 100 μm. Viability was determined with a trypan blue exclusion assay. Apoptosis was measured with a TUNEL assay. $*P \leq 0.05$. DAPI, 4′,6-diamidino-2-phenylindole; DYRK1A, dual-specificity tyrosine phosphorylation-regulated kinase 1A; mRNA, messenger RNA; NS, not significant; pH3, phosphorylated histone H3; PI, propidium iodide; TUNEL, terminal deoxynucleotidyl transferase dUTP nick end labeling. Color images available online at www.liebertpub.com/scd

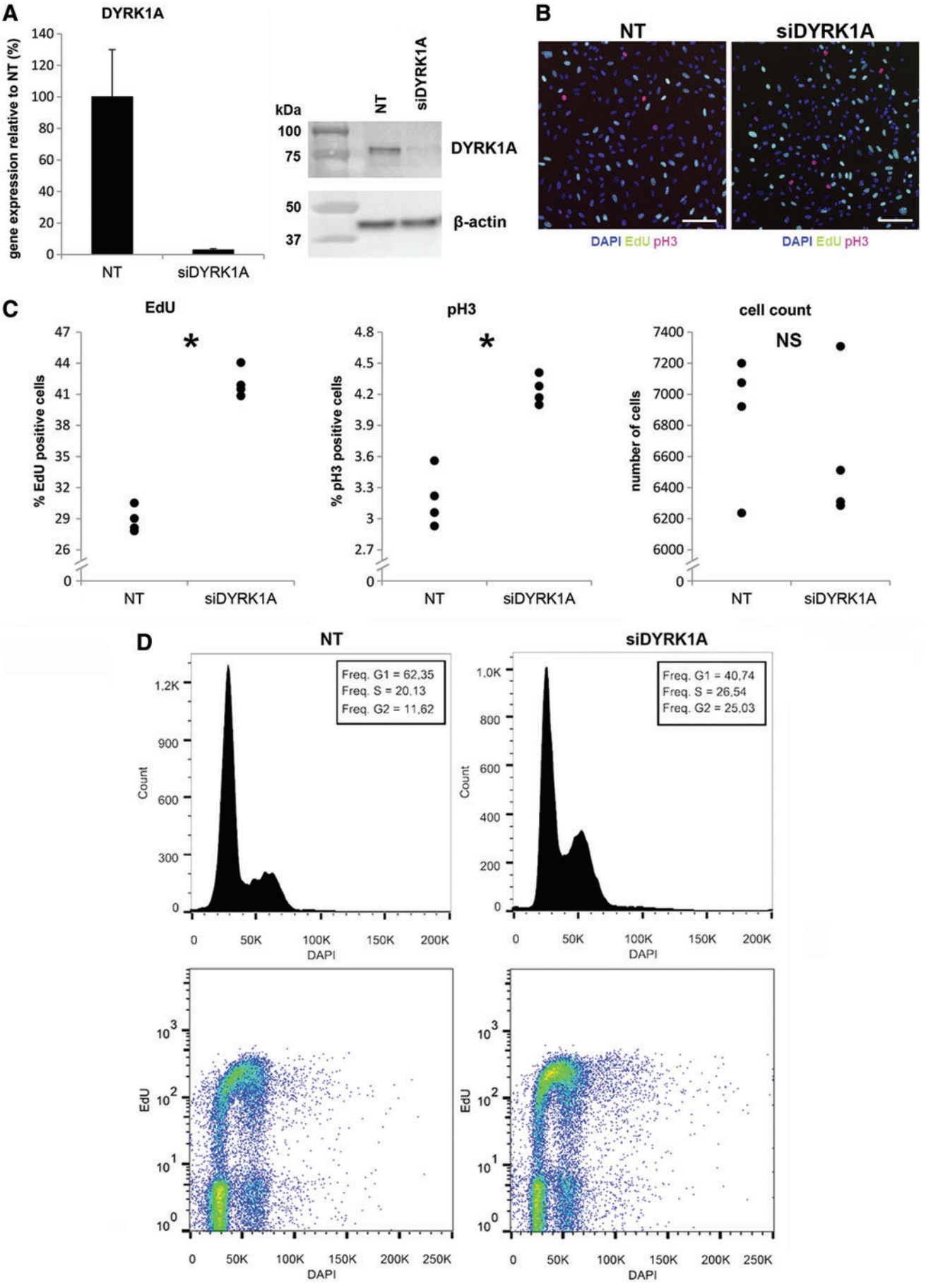

(continued)

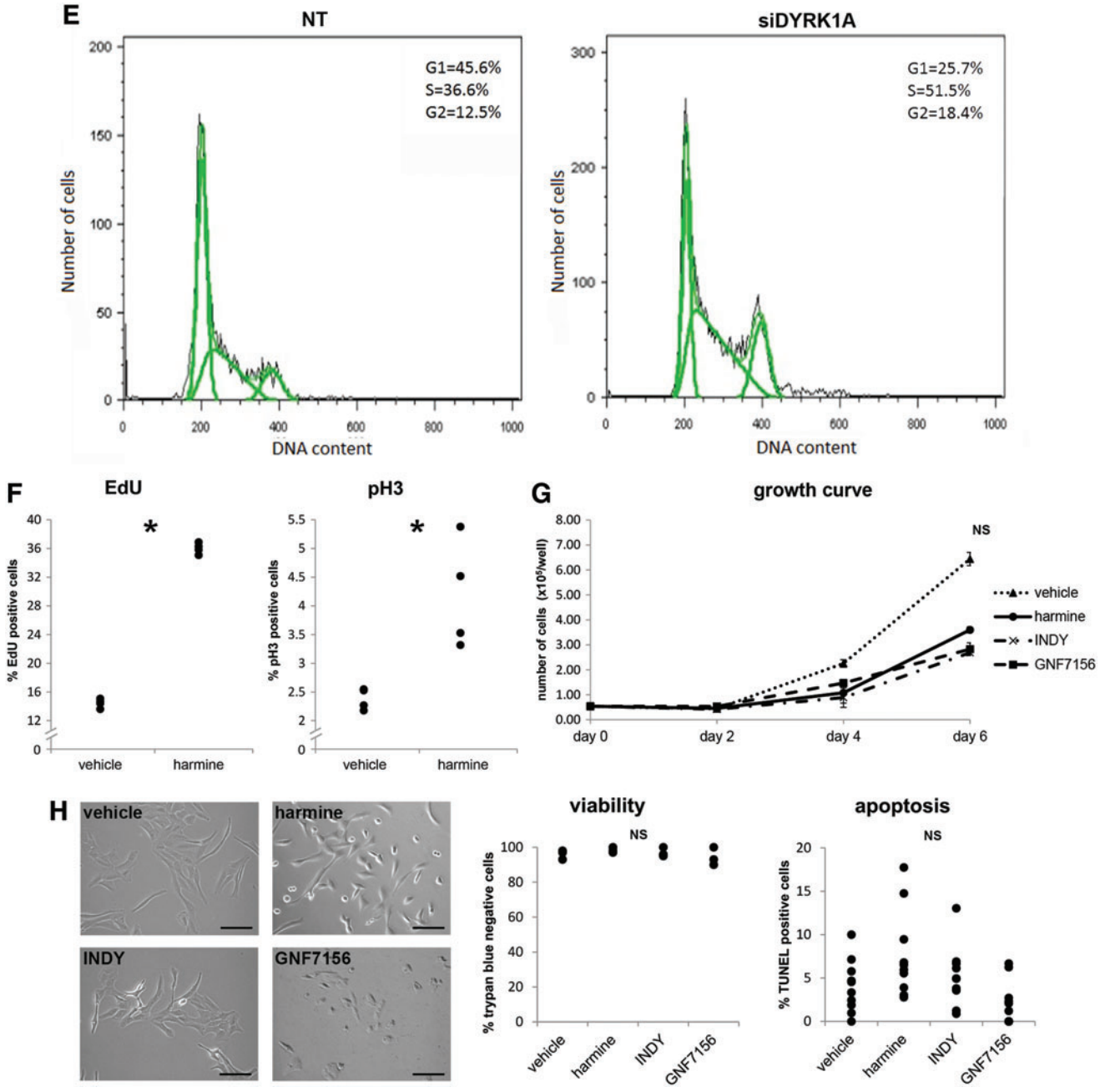

FIG. 3. (Continued).

FIG. 4. Effects of DYRK1A inhibition on liver organoids. **(A)** *Dot* plot of percentage of EdU^+ cells in liver organoids after 48 h of treatment with either vehicle or harmine. *Dots* represent counted organoid sections ($n = 16$ per condition), at least 2,000 nuclei were counted per condition. **(B)** Growth curve of organoids treated with either vehicle or harmine ($n = 4$ culture replicates per condition) as measured with an Alamar Blue assay on the same wells on consecutive days. Serial luminescence measurements were normalized to day 1 (100%). **(C)** *Dot* plot of percentage γH2AX positive cells indicative of DNA damage in liver organoids after 72 h of treatment with either vehicle or harmine. *Dots* represent counted organoid sections ($n = 16$ per condition), at least 1,000 nuclei were counted per condition. **(D)** Western blot for LIN52 (13 kDa) in lysates of HepaRG cells treated with harmine or vehicle control ($n = 3$) and after λPP treatment. The upper band represents the phosphorylated LIN52 (p-LIN52) protein and the lower band the unphosphorylated protein. Sample p-LIN52 was quantified as optical density per mm^2 and normalized against alpha-tubulin. **(E)** *Dot* plots representing relative normalized expression of early (*E2f1*, *Cdc6*, *Pcna*) and late (*Ccnb1*, *Plk1*, *Ect2*) cell cycle progression genes in liver organoids treated with either vehicle or harmine ($n = 4$–6 culture replicates per condition). **(F)** *Dot* plot representing relative normalized expression of cell cycle inhibitor *Cdkn1b* in liver organoids treated with either vehicle or harmine ($n = 4$–6 culture replicates per condition). $^*P \leq 0.05$. λPP, lambda protein phosphatase; AU, arbitrary units; *Ccnb1*, cyclin B1; *Cdc6*, cell division cycle 6; *Cdkn1b*, cyclin-dependent kinase inhibitor 1B; *E2f1*, E2f transcription factor 1; *Ect2*, epithelial cell transforming 2; *Pcna*, proliferating cell nuclear antigen.

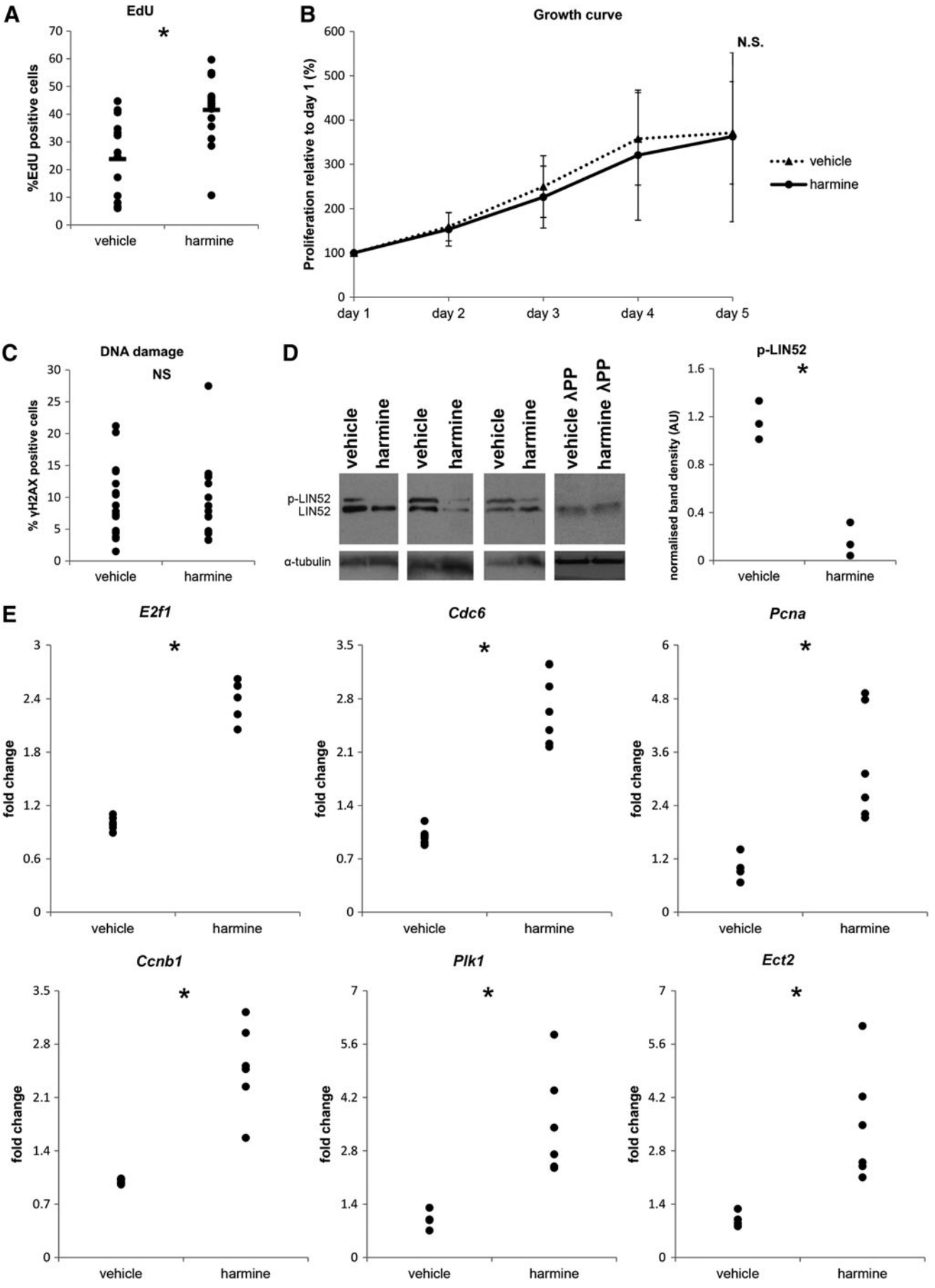

(continued)

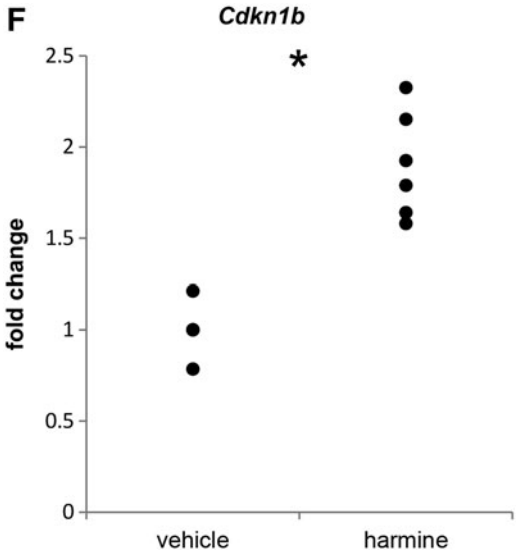

FIG. 4. (Continued).

delay in G2-M-phase progression. The increased S-phase entry upon DYRK1A inhibition is specific for a HPC cell line, because it does not occur in HepG2 or Huh7 cells (well-differentiated hepatocellular tumor cell lines) nor in LX2 cells (hepatic stellate cell line; data not shown). Although it has many hepatic progenitor features and intact p53, the HepaRG is a tumor cell line. Therefore, we asked if DYRK1A would have similar functions in primary HPCs. We utilized organoid technology to evaluate the effects of DYRK1A inhibition on proliferation in primary HPCs, cultured as liver organoids [21].

Effect of DYRK1A inhibition in liver organoids on EdU positivity and proliferation

Liver organoids were treated with either vehicle or harmine and then pulsed with EdU for 6 h. Also in liver organoids, DYRK1A inhibition with harmine resulted in more EdU^+ cells compared with vehicle control (Fig. 4A). Again, harmine treatment did not increase overall proliferation of liver organoids over the course of 5 days, as measured by Alamar Blue assay (Fig. 4B). Unscheduled entry of cells into S phase may result in replication stress and DNA damage. Therefore, we stained cells with the DNA damage marker γH2AX after 72 h of harmine treatment. However, we did not observe a difference, suggesting that DNA damage cannot explain the cell cycle perturbation of DYRK1A-inhibited cells (Fig. 4C).

LIN52 phosphorylation upon DYRK1A inhibition

An earlier study in cell lines by Litovchick et al. demonstrated that DYRK1A-mediated phosphorylation of LIN52 inhibits S-phase entry from a quiescent state through assembly of the Dimerization Partner, RB-like, E2F, and multivulva class B (DREAM) complex [32,33]. This protein complex represses numerous cell cycle genes [34]. We asked whether this function of DYRK1A would underlie the phenotypes we observed in HPCs, and more specifically, if DYRK1A inhibition would affect LIN52 phosphorylation. We performed a western blot for LIN52, which yielded two bands, the upper band represents the phosphorylated LIN52 protein and the lower band the unphosphorylated, and therefore faster migrating LIN52. Chemical inhibition of DYRK1A in HepaRG cells resulted in less phospho-LIN52 and more unphosphorylated LIN52 (Fig. 4D).

Impaired DREAM complex formation would facilitate S-phase entry and cell cycle progression. Transcriptional analysis of liver organoids showed that DYRK1A inhibition increased the expression of genes associated with G1 and early S phase (*E2f1*, *Cdc6*, *Pcna*) as well as late S, G2, and mitotic progression (*Ccnb1*, *Plk1*, *Ect2*) (Fig. 4E). Importantly, these genes are known to be transcriptionally repressed by the DREAM complex [34]. Expression of *Cdkn1b* was induced upon treatment with harmine (Fig. 4F). Together, these data indicate that DYRK1A inhibition decreases LIN52 phosphorylation, resulting in disassembly of the DREAM complex and subsequent upregulation of DREAM target genes and forced S-phase entry in HPCs.

Effect of DYRK1A overexpression in liver organoids on EdU positivity and proliferation

Previous work showed that the effects of *DYRK1A* are highly dependent on gene dosage, as both haploinsufficiency and the presence of an extra copy of the *DYRK1A* gene have been described to affect proliferation in neural progenitor cells [30,35]. We hypothesized that an overexpression of *DYRK1A* in HPCs would impair S-phase entry and as a result decrease proliferation. To answer this question, liver organoid cultures were established from mBACtgDyrk1A mice, which harbor one extra copy of the murine *Dyrk1a* gene (*Dyrk*+++), and their WT littermates. From both WT and *Dyrk*+++, mouse livers biliary duct fragments could be isolated, and after 2–5 days, organoids appeared in the cultures. However, the growth of *Dyrk*+++ organoids was reduced compared to WT cultures (Fig. 5A). qPCR showed that the liver organoids derived from *Dyrk*+++ mice showed a 1.67-fold increase in *Dyrk1a* transcripts consistent with one extra allele of this gene (Fig. 5B). Proliferation was quantified with growth curves and was significantly reduced in *Dyrk*+++ organoids compared with WT organoids (Fig. 5C).

To study S phase entry, WT and *Dyrk*+++ organoids were pulsed with EdU for 3 h. *Dyrk*+++ organoids had a significantly lower percentage of EdU^+ cells compared with WT organoids. Treatment of Dyrk+++ organoids with a DYRK1A inhibitor increased the percentage of EdU^+ cells to WT levels (Fig. 5D). Thus, one extra allele of *Dyrk1a* is sufficient to decrease S-phase entry and proliferation of primary HPCs.

Discussion

Our screen is an unbiased search for intracellular mechanisms in HPC proliferation and reveals *DYRK1A* as essential kinase in the negative regulation of S-phase entry in HPCs. Moreover, an exact gene dosage of *DYRK1A* proved to be crucial, as both silencing and 1.5-fold overexpression perturbed HPC cell cycle progression.

Our study is in line with previous work showing that *DYRK1A* plays a particularly important role in tissue-specific stem cells. However, the consequences of *DYRK1A*

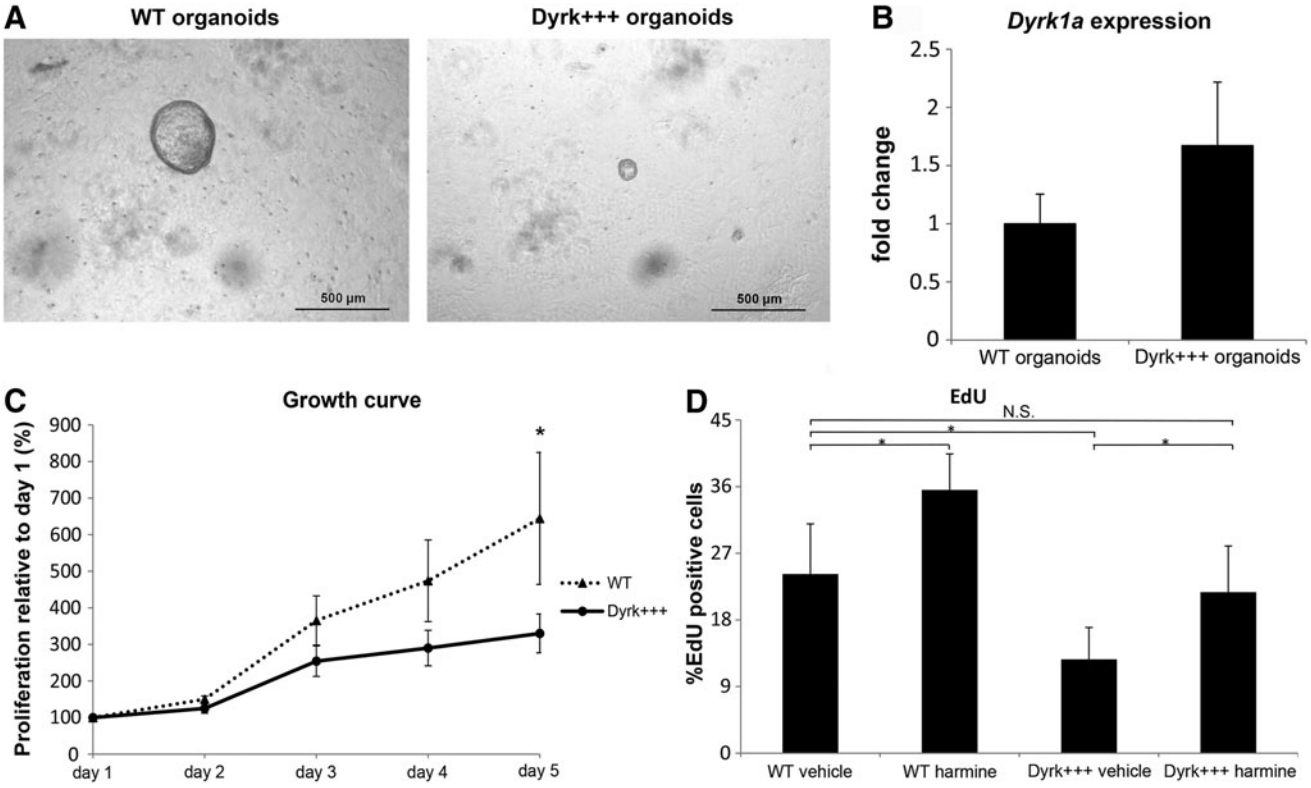

FIG. 5. Effects of DYRK1A overexpression in liver organoids on EdU positivity and proliferation. **(A)** Representative phase contrast images of liver organoids cultured from mBACtgDyrk1A mice, which harbor one extra copy of the murine *Dyrk1a* gene (Dyrk+++), and their WT littermates. Images were taken 7 days after duct isolation. **(B)** Relative normalized gene expression of *Dyrk1a* in liver organoids cultured from WT ($n=5$ donors) and Dyrk+++ ($n=4$ donors) mice, showing a 1.67-fold *Dyrk1a* overexpression. **(C)** Growth curve of WT and Dyrk+++ organoids ($n=4$ culture replicates per genotype) as measured with an Alamar Blue assay on the same wells on consecutive days. Serial luminescence measurements were normalized to day 1 (100%). Representative curve is shown for three WT versus Dyrk+++ donor cultures. **(D)** Percentage of EdU^+ cells in WT and Dyrk+++ liver organoids after 48 h of treatment with either vehicle or harmine. At least 3,500 nuclei were counted per condition (divided over 12 sections per condition). $^*P \leq 0.05$. WT, wild type.

perturbation seem organ-specific. *DYRK1A* was initially discovered as the human homolog of the Drosophila minibrain (*mnb*) gene, involved in neurogenesis [36,37]. In neural progenitors, strict regulation of *DYRK1A* activity is essential for appropriate function, since both, in case of one extra copy and in case of a *DYRK1A* knockout, neurodegenerative and cognitive disorders develop. We found that inhibition of DYRK1A in HPCs increased S phase entry, but did not enhance proliferation. *Dyrk1a* haploinsufficiency in mice results in decreased size of certain brain areas [38]. Inactivating *DYRK1A* mutations in humans is associated with mental retardation and microcephaly [39,40]. *Mnb/Dyrk1a* loss of function in developing chick spinal cord results not only in an increased percentage of $BrdU^+$ and mitotic cells but also in increased apoptosis [30]. We also observed an increased percentage of EdU^+ and $pH3^+$ cells, but neither an increased cell number nor decreased cell viability upon DYRK1A inhibition in either HepaRG cells or organoids, which could be explained by a subsequent delay in G2-M-phase progression.

Interestingly, the effect of DYRK1A perturbation is partly similar in pancreatic cells. The DYRK1A inhibitor harmine was discovered in a chemical screen as an activator of rat and human pancreatic β cell replication, a cell type that is predominantly quiescent [31]. Chemical inhibition of DYRK1A increased β cell BrdU and Ki67 labeling, both in vitro and in vivo. This is in agreement with our findings in HPCs. However, the study also described an induction of β cell proliferation, based on increased β cell mass upon partial pancreatectomy and concurrent treatment with harmine in mice. In addition, harmine treatment improved glycemic control in two mouse models after human pancreatic islet transplantation. A confounding factor to this antidiabetic effect could have been the agonistic effect of harmine on PPARgamma, that was previously shown to improve glucose tolerance and response to insulin in diabetic mice by itself [41]. However, our results strongly suggest that in HPCs, DYRK1A inhibition does not enhance proliferation. Its inactivation did not elicit a proproliferative effect, despite increased S-phase entry and gene expression of various cell cycle markers. Treatment with chemical DYRK1A inhibitors at concentrations that were reported to induce proliferation of neural progenitor cells (INDY) and pancreatic β cells (GNF7156) did not induce HPC proliferation [42,43]. Rather, carefully balanced DYRK1A activity appears to play an important role in coordinating S-phase entry of HPCs.

In line with this, we found that overexpression of *DYRK1A* in HPCs decreased S-phase entry and decreased proliferation. Similarly, in embryonic mouse brain and chick spinal cord, *Dyrk1a* overexpression resulted in proliferation arrest of neural progenitors [30,35]. This was confirmed by Park et al. who found that *DYRK1A* overexpression resulted in attenuated proliferation of human embryonic stem cell-derived neural precursors [29]. *DYRK1A* is located on the Down Syndrome critical region of chromosome 21 and is considered to contribute to abnormal brain development and mental retardation in human Down Syndrome [29,44]. To evaluate whether the phenotype we observed is specific for HPCs, we also studied other liver cell lines (stellate cells, hepatocytes), but did not observe the same effect of DYRK1A inhibition on the cell cycle.

Previous publications have reported on a role of DYRK1A in cell cycle progression based on interaction with the DREAM (DP, RB, E2F, and MuvB) complex [32,33,45]. DYRK1A can phosphorylate LIN52, a subunit of the MuvB core, which is necessary for DREAM complex assembly and entry into a quiescent state. When DYRK1A-mediated phosphorylation of LIN52 is blocked, the MuvB core dissociates from the DREAM complex and binds to MYB (MMB complex) to initiate cell cycle entry. Transcriptional analysis has indicated that the DREAM complex can repress transcription of genes in both early (G1/S) and late (G2/M) cell cycle progression [34]. MMB target genes are transcriptionally activated and are mainly involved in G2/M phase of the cell cycle. We found that chemical inhibition of DYRK1A decreased LIN52 phosphorylation in HPCs, which would impair DREAM and favor MMB complex formation. Indeed, in harmine-treated HPCs expression of early cell cycle DREAM target genes *E2f1*, *Cdc6*, and *Pcna* was upregulated as well as the expression of late cell cycle MMB target genes *Ccnb1*, *Plk1*, and *Ect2*. Other studies have indicated DYRK1A-mediated effects on the cell cycle through regulation of nuclear factor of activated T-cells (*NFAT*) signaling [46] and through induction of *Cdkn1b* [30]. Whether these mechanisms also play a role in HPC proliferation warrants further investigation. *Nfatc1* and *Nfatc2* gene expression is detectable in primary HPCs, but at very low levels (data not shown). Inhibition of DYRK1A did not downregulate expression of *Cdkn1b* in HPCs, but rather increased *Cdkn1b* levels.

There are a few limitations to our study. To reduce variation, the siRNA screen was performed in a cell line, which is naturally transformed and, hence, may not fully represent HPCs in vivo. This limitation could largely be overcome by including primary HPCs as a biological validation of obtained hits. Second, we chose to focus our screen to a kinase library, because kinases are known for their involvement in proliferation and are potential drug targets. Third, we exerted quite a stringent hit validation approach to select only for true positive hits. However, this strategy could have resulted in false negatives.

In conclusion, we found an essential role of *DYRK1A* as regulator of cell cycle progression in cultured HPCs. A possible mechanism is through interference with DREAM and MMB complex formation, involved in S-phase entry from a G0 quiescent state. Future research may focus on upstream regulation of *DYRK1A* transcription and activity in HPCs and other downstream effector mechanisms of DYRK1A phosphorylation targets. Knowledge gained in these studies can contribute to our understanding of HPC quiescence and activation and may provide tools to enhance HPC-mediated liver regeneration during severe liver disease.

Acknowledgments

This study was funded by the Netherlands Organization for Scientific Research NWO ZON/MW (116004121). The authors thank Daphne Lelieveld and Dr. Sathidpak Nantasanti for technical assistance, Balaji Ramalingam for data analysis, and Prof. Scott Friedman for providing the LX2 cell line.

Author Disclosure Statement

No competing financial interests exist.

References

1. Higgins GM and RM Anderson. (1931). Experimental pathology of the liver. I. Restoration of the liver of the white rat following partial surgical removal. Arch Pathol 12:186–202.
2. Riehle KJ, YY Dan, JS Campbell and N Fausto. (2011). New concepts in liver regeneration. J Gastroenterol Hepatol 26 (Suppl. 1):203–212.
3. Katoonizadeh A, F Nevens, C Verslype, J Pirenne and T Roskams. (2006). Liver regeneration in acute severe liver impairment: a clinicopathological correlation study. Liver Int 26:1225–1233.
4. Lunz JG, 3rd, H Tsuji, I Nozaki, N Murase and AJ Demetris. (2005). An inhibitor of cyclin-dependent kinase, stress-induced p21Waf-1/Cip-1, mediates hepatocyte mitoinhibition during the evolution of cirrhosis. Hepatology 41: 1262–1271.
5. Liu L, GR Yannam, T Nishikawa, T Yamamoto, H Basma, R Ito, M Nagaya, J Dutta-Moscato, DB Stolz, et al. (2012). The microenvironment in hepatocyte regeneration and function in rats with advanced cirrhosis. Hepatology 55: 1529–1539.
6. Roskams T, R De Vos, P Van Eyken, H Myazaki, B Van Damme and V Desmet. (1998). Hepatic OV-6 expression in human liver disease and rat experiments: evidence for hepatic progenitor cells in man. J Hepatol 29:455–463.
7. Lowes KN, BA Brennan, GC Yeoh and JK Olynyk. (1999). Oval cell numbers in human chronic liver diseases are directly related to disease severity. Am J Pathol 154:537–541.
8. Libbrecht L, D Cassiman, V Desmet and T Roskams. (2001). Expression of neural cell adhesion molecule in human liver development and in congenital and acquired liver diseases. Histochem Cell Biol 116:233–239.
9. Tan J, P Hytiroglou, R Wieczorek, YN Park, SN Thung, B Arias and ND Theise. (2002). Immunohistochemical evidence for hepatic progenitor cells in liver diseases. Liver 22:365–373.
10. Boulter L, O Govaere, TG Bird, S Radulescu, P Ramachandran, A Pellicoro, RA Ridgway, SS Seo, B Spee, et al. (2012). Macrophage-derived Wnt opposes Notch signaling to specify hepatic progenitor cell fate in chronic liver disease. Nat Med 18:572–579.
11. Gouw AS, AD Clouston and ND Theise. (2011). Ductular reactions in human liver: diversity at the interface. Hepatology 54:1853–1863.

12. Orford KW and DT Scadden. (2008). Deconstructing stem cell self-renewal: genetic insights into cell-cycle regulation. Nat Rev Genet 9:115–128.
13. Fuchs E and T Chen. (2013). A matter of life and death: self-renewal in stem cells. EMBO Rep 14:39–48.
14. Spee B, G Carpino, BA Schotanus, A Katoonizadeh, S Vander Borght, E Gaudio and T Roskams. (2010). Characterisation of the liver progenitor cell niche in liver diseases: potential involvement of Wnt and Notch signalling. Gut 59:247–257.
15. Ishikawa T, VM Factor, JU Marquardt, C Raggi, D Seo, M Kitade, EA Conner and SS Thorgeirsson. (2012). Hepatocyte growth factor/c-met signaling is required for stem-cell-mediated liver regeneration in mice. Hepatology 55: 1215–1226.
16. Tirnitz-Parker JE, CS Viebahn, A Jakubowski, BR Klopcic, JK Olynyk, GC Yeoh and B Knight. (2010). Tumor necrosis factor-like weak inducer of apoptosis is a mitogen for liver progenitor cells. Hepatology 52:291–302.
17. Kallis YN, AJ Robson, JA Fallowfield, HC Thomas, MR Alison, NA Wright, RD Goldin, JP Iredale and SJ Forbes. (2011). Remodelling of extracellular matrix is a requirement for the hepatic progenitor cell response. Gut 60:525–533.
18. Rauch J, N Volinsky, D Romano and W Kolch. (2011). The secret life of kinases: functions beyond catalysis. Cell Commun Signal 9:23.
19. Lindqvist A, V Rodriguez-Bravo and RH Medema. (2009). The decision to enter mitosis: feedback and redundancy in the mitotic entry network. J Cell Biol 185:193–202.
20. Garnier D, P Loyer, C Ribault, C Guguen-Guillouzo and A Corlu. (2009). Cyclin-dependent kinase 1 plays a critical role in DNA replication control during rat liver regeneration. Hepatology 50:1946–1956.
21. Huch M, C Dorrell, SF Boj, JH van Es, VS Li, M van de Wetering, T Sato, K Hamer, N Sasaki, et al. (2013). In vitro expansion of single $Lgr5^+$ liver stem cells induced by Wnt-driven regeneration. Nature 494:247–250.
22. Guedj F, PL Pereira, S Najas, MJ Barallobre, C Chabert, B Souchet, C Sebrie, C Verney, Y Herault, M Arbones and JM Delabar. (2012). DYRK1A: a master regulatory protein controlling brain growth. Neurobiol Dis 46:190–203.
23. Salic A and TJ Mitchison. (2008). A chemical method for fast and sensitive detection of DNA synthesis in vivo. Proc Natl Acad Sci U S A 105:2415–2420.
24. Birmingham A, LM Selfors, T Forster, D Wrobel, CJ Kennedy, E Shanks, J Santoyo-Lopez, DJ Dunican, A Long, et al. (2009). Statistical methods for analysis of high-throughput RNA interference screens. Nat Methods 6: 569–575.
25. Simpson KJ, LM Selfors, J Bui, A Reynolds, D Leake, A Khvorova and JS Brugge. (2008). Identification of genes that regulate epithelial cell migration using an siRNA screening approach. Nat Cell Biol 10:1027–1038.
26. van Steenbeek FG, L Van den Bossche, GC Grinwis, A Kummeling, IH van Gils, MJ Koerkamp, D van Leenen, FC Holstege, LC Penning, et al. (2013). Aberrant gene expression in dogs with portosystemic shunts. PLoS One 8: e57662.
27. Adayev T, J Wegiel and YW Hwang. (2011). Harmine is an ATP-competitive inhibitor for dual-specificity tyrosine phosphorylation-regulated kinase 1A (Dyrk1A). Arch Biochem Biophys 507:212–218.
28. Gockler N, G Jofre, C Papadopoulos, U Soppa, FJ Tejedor and W Becker. (2009). Harmine specifically inhibits protein kinase DYRK1A and interferes with neurite formation. FEBS J 276:6324–6337.
29. Park J, Y Oh, L Yoo, MS Jung, WJ Song, SH Lee, H Seo and KC Chung. (2010). Dyrk1A phosphorylates p53 and inhibits proliferation of embryonic neuronal cells. J Biol Chem 285:31895–31906.
30. Hammerle B, E Ulin, J Guimera, W Becker, F Guillemot and FJ Tejedor. (2011). Transient expression of Mnb/Dyrk1a couples cell cycle exit and differentiation of neuronal precursors by inducing p27KIP1 expression and suppressing NOTCH signaling. Development 138:2543–2554.
31. Wang P, JC Alvarez-Perez, DP Felsenfeld, H Liu, S Sivendran, A Bender, A Kumar, R Sanchez, DK Scott, A Garcia-Ocaña and AF Stewart. (2015). A high-throughput chemical screen reveals that harmine-mediated inhibition of DYRK1A increases human pancreatic beta cell replication. Nat Med 21:383–388.
32. Litovchick L, S Sadasivam, L Florens, X Zhu, SK Swanson, S Velmurugan, R Chen, MP Washburn, XS Liu and JA DeCaprio. (2007). Evolutionarily conserved multisubunit RBL2/p130 and E2F4 protein complex represses human cell cycle-dependent genes in quiescence. Mol Cell 26: 539–551.
33. Litovchick L, LA Florens, SK Swanson, MP Washburn and JA DeCaprio. (2011). DYRK1A protein kinase promotes quiescence and senescence through DREAM complex assembly. Genes Dev 25:801–813.
34. Fischer M, P Grossmann, M Padi and JA DeCaprio. (2016). Integration of TP53, DREAM, MMB-FOXM1 and RB-E2F target gene analyses identifies cell cycle gene regulatory networks. Nucleic Acids Res 44:6070–6086.
35. Yabut O, J Domogauer and G D'Arcangelo. (2010). Dyrk1A overexpression inhibits proliferation and induces premature neuronal differentiation of neural progenitor cells. J Neurosci 30:4004–4014.
36. Tejedor F, XR Zhu, E Kaltenbach, A Ackermann, A Baumann, I Canal, M Heisenberg, KF Fischbach and O Pongs. (1995). minibrain: A new protein kinase family involved in postembryonic neurogenesis in *Drosophila*. Neuron 14: 287–301.
37. Shindoh N, J Kudoh, H Maeda, A Yamaki, S Minoshima, Y Shimizu and N Shimizu. (1996). Cloning of a human homolog of the *Drosophila minibrain*/rat Dyrk gene from ''the Down syndrome critical region'' of chromosome 21. Biochem Biophys Res Commun 225:92–99.
38. Fotaki V, M Dierssen, S Alcantara, S Martinez, E Marti, C Casas, J Visa, E Soriano, X Estivill and ML Arbonés. (2002). Dyrk1A haploinsufficiency affects viability and causes developmental delay and abnormal brain morphology in mice. Mol Cell Biol 22:6636–6647.
39. Moller RS, S Kubart, M Hoeltzenbein, B Heye, I Vogel, CP Hansen, C Menzel, R Ullmann, N Tommerup, et al. (2008). Truncation of the Down syndrome candidate gene DYRK1A in two unrelated patients with microcephaly. Am J Hum Genet 82:1165–1170.
40. van Bon BW, A Hoischen, J Hehir-Kwa, AP de Brouwer, C Ruivenkamp, AC Gijsbers, CL Marcelis, N de Leeuw, JA Veltman, HG Brunner and BB de Vries. (2011). Intragenic deletion in DYRK1A leads to mental retardation and primary microcephaly. Clin Genet 79:296–299.

41. Waki H, KW Park, N Mitro, L Pei, R Damoiseaux, DC Wilpitz, K Reue, E Saez and P Tontonoz. (2007). The small molecule harmine is an antidiabetic cell-type-specific regulator of PPARgamma expression. Cell Metab 5:357–370.
42. Dakic V, RM Maciel, H Drummond, JM Nascimento, P Trindade and SK Rehen. (2016). Harmine stimulates proliferation of human neural progenitors. PeerJ 4:e2727.
43. Shen W, B Taylor, Q Jin, V Nguyen-Tran, S Meeusen, YQ Zhang, A Kamireddy, A Swafford, AF Powers, et al. (2015). Inhibition of DYRK1A and GSK3B induces human β-cell proliferation. Nat Commun 6:8372.
44. Kurabayashi N and K Sanada. (2013). Increased dosage of DYRK1A and DSCR1 delays neuronal differentiation in neocortical progenitor cells. Genes Dev 27:2708–2721.
45. Boichuk S, JA Parry, KR Makielski, L Litovchick, JL Baron, JP Zewe, A Wozniak, KR Mehalek, N Korzeniewski, et al. (2013). The DREAM complex mediates GIST cell quiescence and is a novel therapeutic target to enhance imatinib-induced apoptosis. Cancer Res 73: 5120–5129.
46. Gwack Y, S Sharma, J Nardone, B Tanasa, A Iuga, S Srikanth, H Okamura, D Bolton, S Feske, PG Hogan and A Rao. (2006). A genome-wide *Drosophila* RNAi screen identifies DYRK-family kinases as regulators of NFAT. Nature 441:646–650.

Address correspondence to:
Hedwig S. Kruitwagen, DVM, PhD
Department of Clinical Sciences of Companion Animals
Faculty of Veterinary Medicine
Utrecht University
Yalelaan 104
3584 CM Utrecht
The Netherlands

E-mail: h.s.kruitwagen@uu.nl

Received for publication July 4, 2017
Accepted after revision November 27, 2017
Prepublished on Liebert Instant Online November 28, 2017